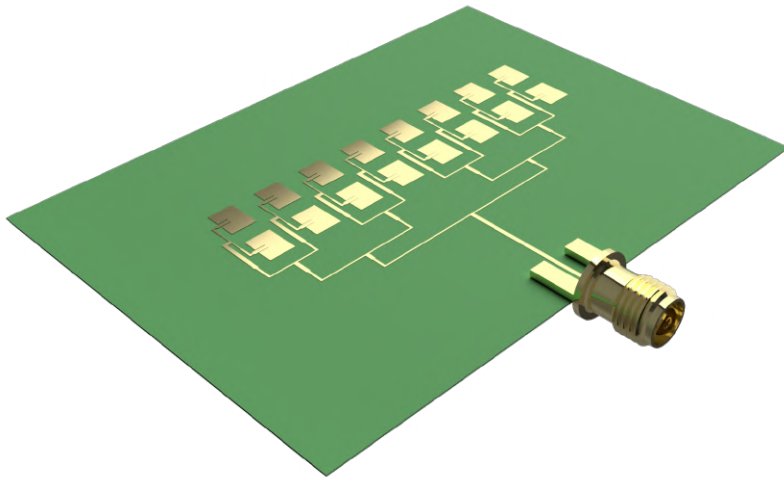**Bachelor Thesis**

Antenna for RADAR Ground Speed Sensor

Author   Rafael Riber

Supervision   Prof. Anja Skrivervik, Dr. Germán A. Ramírez A. Ph.D
Microwaves and Antennas Group

Contents

List of Figures

List of Tables

Abbreviations

ADAS Advanced Driver Assistance Systems

ADC Analog-to-digital converter

AF Array Factor

AUT Antenna Under Test

CAN Controller Area Network

GNSS Global navigation satellite system

HPBW Half Power Beam Width

MCU Microcontroller Unit

MMIC Monolithic microwave integrated circuit

PCB Printed Circuit Board

PHY Physical Layer

RADAR Radio Detection And Ranging

RTK Real-time kinematic positioning

RF Radio Frequency

RX Receive

SSFIP Strip-Slot-Foam-Inverted-Patch

SLL Sidelobe Level

SoG Speed over ground

TX Transmit

1 Introduction

Doppler Radio Detection And Ranging (RADAR) can be used to measure the speed of targets, and reciprocally the relative speed between a vehicle and the ground. This idea has existed for as far back as the 1940s, but was at first only used for military purposes [5] and the technology had not reached a point where miniaturization not only of the Radio Frequency (RF) circuitry but also of the signal processing units was possible.

In more recent years with the democratization and miniaturization of such systems with the development of Advanced Driver Assistance Systems (ADAS) and other autonomous driving technologies, RADAR is used for many applications in the automotive industry, mainly for collision detection and avoidance and even imaging radar for autonomous vehicles.

In this project, an antenna for a RADAR vehicle speed measurement system (also called Speed over ground (SoG) sensor [4]) is designed and characterized, taking into consideration several aspects such as overall system architecture and mounting in order to limit speed measurement errors induced by the antenna.

1.1 Motivation

The main motivation for this project was the need of a precise speed measurement of EPFL Racing Team's Formula Student vehicles, with the recent introduction of different control technologies such as traction control and torque vectoring in the team's vehicles, and the development of driverless capabilities all requiring as good a measurement of the vehicle's speed relative to the ground as possible, regardless of wheel slippage. Comparing different systems, RADAR is as we will see an interesting option not only for precision reasons but also for cost, weight and ruggedness purposes, and can contribute as an additionnal source of speed measurement for use with sensor fusion algorithms.

1.2 Speed measurement medium comparison

There exists many ways to measure the speed of a vehicle, the first one being measuring the rotation speed of the wheels with encoders. This can however lead to an error in measurement due to the wheels slipping and their rotational speed being related to the vehicle's speed by complex tire models. Although this is less of an issue in production vehicles, it can become an issue in performance electric race cars such as EPFL Racing Team's Formula Student vehicles, capable of accelerating to 100 km/h in under 3 seconds. Under a high acceleration, wheel slippage is almost certain and becomes an issue when using the wheel speed as a measure of the vehicle speed for control algorithms. To be able to accurately measure speed and guarantee the proper function of control algorithms, several options exist and a comparison between them is shown in table 1. The most common method is Global navigation satellite system (GNSS), that can measure speeds accurately and is already present in production vehicles and implemented in most Formula Student vehicles. A more precise version of GNSS called Real-time kinematic positioning (RTK) is being implemented in the newest EPFL Racing Team vehicle and proves to be extremely accurate, but at the expense of weight and cost.

Another option using optical sensors pointing at the ground can also be very effective, and has been explored in previous projects within the team with promising results [15] at a reasonable cost, but quite far from the performance of commercial solutions [16].

Finally, RADAR speed measurement fits quite well within those options, and can have a high accuracy when coupled with good signal processing [6] [4] [2] [1] [9], so the exploration of this option within the team for research and development for future vehicles seemed quite natural.

All these different methods of measurement can be used simultaneously and combined using specific algorithms increase measurement accuracy [17]. Moreover, this can also increase safety since a lower accuracy of one measurement type in certain conditions or outright sensor failure of one type of measurement does not lead to a complete loss of speed awareness.

System	Weight	Cost	Accuracy
GNSS (RTK)	400g	≥ 40K CHF	Extreme (0.01m/s)
Professional Optical Sensor	250g	≥ 10K CHF	Very High (0.1m/s)
Homemade Optical Sensor	100g	150 CHF	High (1.5m/s)
RADAR	100g	200 CHF	High (0.1-1m/s)

Table 1: Comparison of possible Speed Measurement Systems

1.3 Objectives

The main objective of this project is the design, realization and characterization of a Doppler RADAR antenna.

The specific objectives of the project are

- define the antenna technology and architecture.

- design the antenna.

- realize the prototype.

- validate the prototype.

The technical performance requirements of the antenna array are given in terms of the desired performance of the final system, and the specific mounting and configuration requirements of Formula Student [13]. The main performance targets for the full system are the following:

	Acceptable	Ideal
Measurement rate [ms]	100	10
Resolution [m/s]	1	0.1
Range [km/h]	0-50	0-120
Cost [CHF]	400	150

Table 2: Final system performance targets

2 Basic concepts

2.1 Doppler RADAR

Doppler RADAR is one of the simplest forms of RADAR [7, p.340]. It functions based on the Doppler effect, that is commonly known as the apparent change in frequency f_t emitted by a moving source for a fixed observer (f_r). This relationship is the following:

$$f_r = f_t \left(\frac{1 + v/c}{1 - v/c} \right) \tag{2.1}$$

With v the speed of the moving source, f_r the observed frequency, f_t the source frequency and c the speed of light.

The Doppler frequency f_d (also called beat frequency) is defined as:

$$f_d = f_r - f_t = 2v \frac{f_t}{(c - v)} \tag{2.2}$$

Although this effect is commonly used by stationnary RADAR stations to measure the speed of moving targets (usually planes or other flying objects) [18, chap. 17], the reciprocity of the Doppler effect means we can use Doppler RADAR to measure the speed of a vehicle with an on-board RADAR source relative to the ground. From the point of view of the vehicle, this is equivalent to measuring the speed of a moving target.
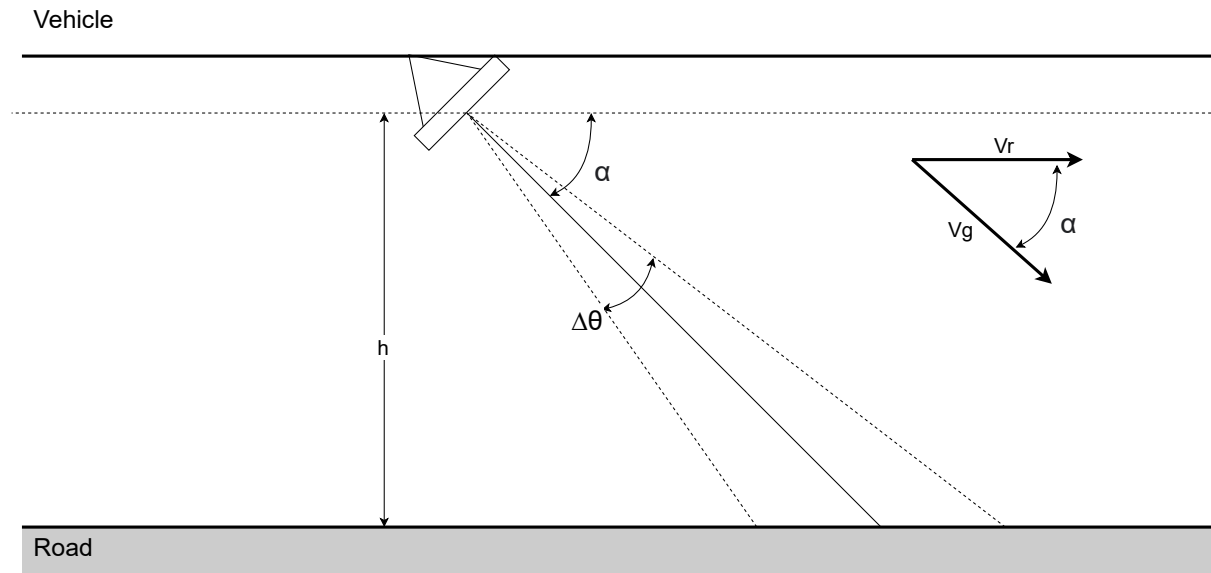
2.2 Problem Geometry

Fig. 1: Problem Geometry

The problem geometry is defined in figure 1. In this configuration, the speed measurement system is mounted on the underside of the vehicle, with direct line of sight of the road surface at a fixed height h, with $h > 30$mm in Formula Student regulations [13].

The degrees of freedom of such a system are the following:

- The mounting height h

- The beam angle α defined as the angle between the velocity vector of magnitude V_g and the center of the antenna beam.

- The Half Power Beam Width (HPBW) $\Delta\theta$ of the antenna in the E-Plane.

The HPBW in the horizontal (H-Plane) axis of the antenna has, as we will see, little effect on measurement accuracy. We can however choose to limit it in order to avoid unwanted reflections as we will see later.

In order to guarantee good accuracy of the overall system, we will now explore the effect of these parameters in order to then design a suitable antenna.

2.3 Doppler Spectrum

The Doppler relationship [5] states that:

$$f_d = f_t\left(1 - \frac{c - V_r}{c + V_r}\right) \approx \frac{2V_r f_t}{c} = \frac{2V_r}{\lambda} \tag{2.3}$$

With V_r the vehicle velocity vector in the direction of travel.

Since $V_r = V_g \cos\alpha$, with V_g the velocity component colinear to the RADAR beam, we get the Doppler frequency

$$f_d = \frac{2V_g}{\lambda}\cos\alpha \tag{2.4}$$

From which we can derive the vehicle speed: $V_r = \frac{f_d \lambda}{2}$

In reality, the Doppler frequency spectrum has a certain spread that is dependent on the characteristics of the antenna [10][11][5]. This spread is given by

$$\Delta f_d = \frac{2V_g}{\lambda}\left[\cos\left(\frac{\alpha - \Delta\theta}{2}\right) - \cos\left(\frac{\alpha + \Delta\theta}{2}\right)\right] \approx \frac{2V_g}{\lambda}\Delta\theta\sin\alpha \tag{2.5}$$

Differentiating equation 2.4 we get the relationship between Δf_d and the speed error ΔV_g

$$\Delta f_d = \frac{2\Delta V_g}{\lambda}\cos\alpha \tag{2.6}$$

Substituting the obtained expression of Δf_d into equation 2.5 we have:

$$\Delta V_g = \frac{V_g}{\cos\alpha}\left[\cos\left(\frac{\alpha - \Delta\theta}{2}\right) - \cos\left(\frac{\alpha + \Delta\theta}{2}\right)\right] \approx \frac{V_g}{\cos\alpha}\Delta\theta\sin\alpha = V_g\Delta\theta\tan\alpha \tag{2.7}$$

And we get the following expression for relative speed error (assuming perfect signal processing, see section 6.1):

$$\frac{\Delta V_g}{V_g} = \Delta\theta\tan\alpha \tag{2.8}$$

As expected, the smaller the HPBW and beam angle, the lowest the error. However in order to avoid reflections on the underside of the vehicle we can set the following further requirement:
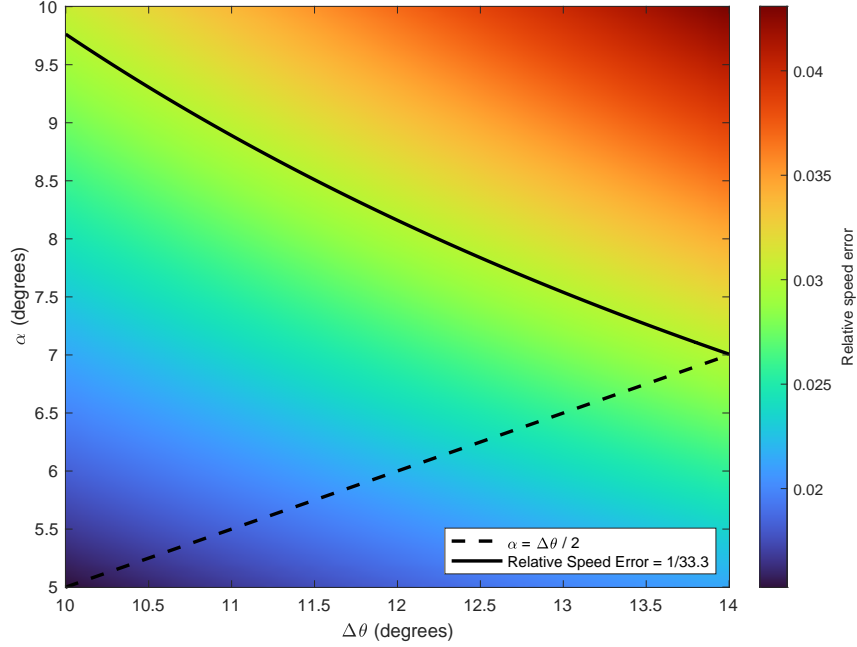
$$\alpha > \frac{\Delta\theta}{2} \tag{2.9}$$

Fig. 2: Relative speed error vs beam width and beam angle

Figure 2 shows the relationship between relative speed error, HPBW and beam angle α. The requirement from equation 2.9 is respected for values above the dashed line, and values under the solid line represent a relative error (eq. 2.8) below 1 m/s at 120 km/h. From this we obtain a better idea of the compromise between beam angle, HPBW and relative error, and it becomes quite clear that the designed antenna should have a HPBW below 14 degrees but as narrow as possible to satisfy both requirements.

We can notice the mounting height h has no influence on the speed error in this model, although it impacts the distance travelled by the RADAR wave significantly and thus the received power level. This must be taken into account when doing the link budget of the overall system, but this is (for now) outside of the scope of the antenna design.

Another aspect to note is the dependence in λ in equation 2.5, which shows that a higher frequency leads to a higher Doppler spread. In fact, doubling the frequency would effectively double the spread, however we can see from equation 2.7 that the speed error is not affected by frequency, since it is also scaled by the frequency and the frequency terms cancel out when substituting equation 2.6 into 2.5. It must however be noted that an unstable operating frequency could cause some additional unwanted errors, therefore a signal source as accurate as possible must be used to mitigate this effect.

3 System Architecture

The overall system architecture must include the following components to be able to derive the vehicle speed:

- A suitable signal source

- A way to derive the Doppler frequency for further processing

- Suitable Transmit (TX) and Receive (RX) antennas

Several manufacturers such as Texas Instruments and Infineon offer Monolithic microwave integrated circuits (MMICs) capable of synthesizing the RADAR signal and deriving the Doppler frequency from the shift between sent and received signal, effectively removing the need for any other integrated RF circuitry. Although the K band (24 GHz) was the standard frequency band for automotive RADAR since it's democratization for ADAS, a recent shift towards a new standard in the W-band (77-81GHz) means the 24 GHz solutions are slowly being phased out for automotive use, since 77GHz allows for smaller systems and advanced capabilities like imaging RADAR. However, for the purposes of this project, a 24 GHz frequency was chosen since measurement facilities were available to characterize the system, and the overall size of the resulting system would not be an issue.

At the time of this project, Infineon's BGT24LTR11 Silicon Germanium 24GHz Radar Transceiver MMIC [14] was readily available, relatively cheap (less than 10 CHF), and integrated all the necessary functions in one package, with single ended TX and RX ports. It also operates at usual microcontroller voltages (3.3V), has a good output power (10 dBm) and is easily integrated with its small size of 2.4x2.4mm. A stable frequency being paramount to good accuracy, it also integrates internal temperature compensating which is another advantage. Based on this component, the following architecture can be designed, with the idea of using the same antenna design for both the TX and RX antennas:
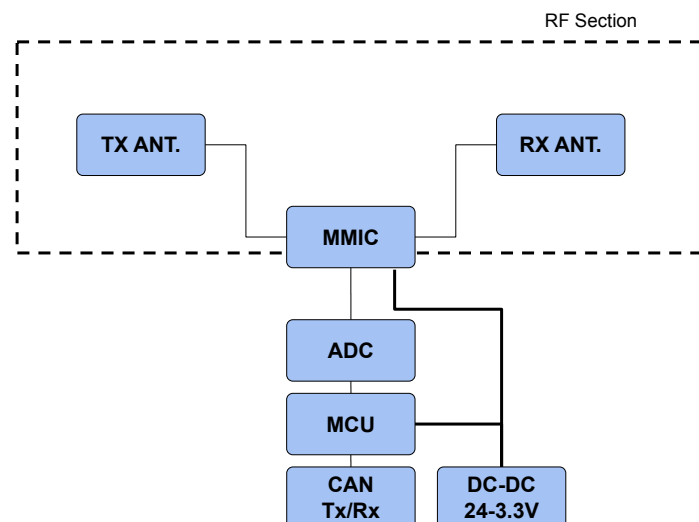

Fig. 3: Overall architecture

The focus of this project being the design of the antenna, only some overall system blocks are included in figure 3, namely the antennas, MMIC, Analog-to-digital converter (ADC) and Microcontroller Unit (MCU) with Controller Area Network (CAN) Physical Layer (PHY) to transmit the computed speed back to the vehicle, and some power circuitry.

4 Antenna Array Design

In order to be implemented into a final system on a Printed Circuit Board (PCB) an inset-fed microstrip patch antenna was chosen for the simplicity of manufacturing and integration with a RADAR MMIC, the fact the desired HPBW can be attained by an array of such elements, and no particular need for a wide bandwidth since the system operates ideally at a constant frequency. This would allow to use the same antenna design for both the TX and RX antennas, and print the whole RF section or even the whole system including a processing unit all on one board. In this section, an array element is designed, and the Array Factor (AF) for a NxM planar array is derived to obtain the desired HPBW as discussed in section 2.3.

4.1 Array element

From available substrates, Rogers RO4003C was chosen because of its good properties at such frequencies. Following the patch antenna formulas from [12, pp.816-820], the following dimensions were calculated for a rectangular patch antenna resonating at 24 GHz on Rogers 4003C substrate:

Substrate Thickness [mm]	Width [mm]	Length [mm]
0.203	4.14	3.25
0.508	4.14	3.08

Table 3: Calculated patch dimensions

Due to substrate availability, the first simulations were run on ANSYS HFSS, using a 0.508 mm substrate, with the 50 Ω trace width W_{50} for this thickness being 1.2mm. However this gave strange results with an asymmetric radiation pattern, possibly due to W_{50} being too close to the patch dimensions (see figure 4).
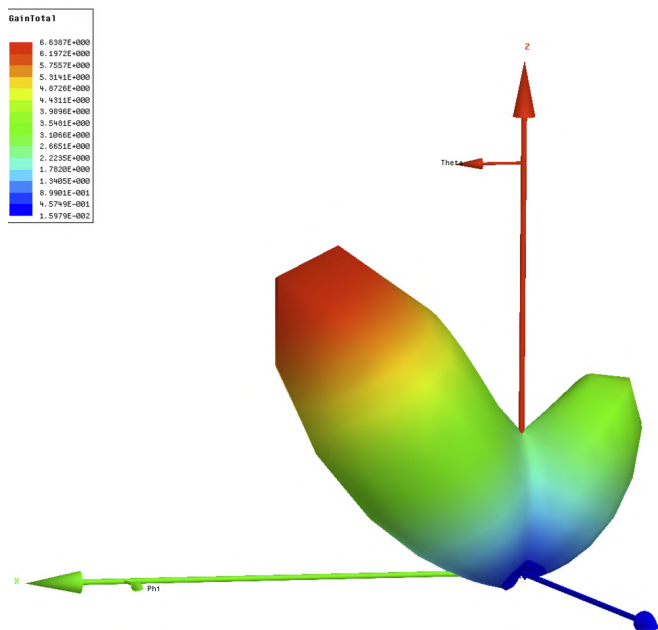

Fig. 4: First simulation with 0.508mm substrate

Although it was possible to adjust the patch dimensions to match the antenna with a -15 dB S_{11}, no adjustments allowed to get an acceptable radiation pattern. To fix this issue, the following actions could be undertaken:

- Changing the feeding method to a coaxial probe feed.

- Changing the antenna element to a Strip-Slot-Foam-Inverted-Patch (SSFIP) to have separate substrate thicknesses for feeding and radiation.

- Choosing a thinner substrate to lower W_{50}.

Due to time constraints and the desire to have the feeding on the same layer as the antenna elements for easier integration, changing the substrate thickness to 0.203mm was attempted first. Setting the patch length to the calculating length and with a patch width lower than the length, the length was tuned from the calculated dimension (3.25mm) to 3.23mm in order to match the antenna to the desired frequency. With promising results, the width was changed to the calculated width of 4.14mm, and the inset feed was adjusted to 1.23mm to have the lowest possible S_{11}.

The obtained element showed satisfactory characteristics (see table 4 and figure 5), and notably a symmetric radiation pattern as expected for a patch antenna.

Peak Directivity [dB]	6.32
Peak Realized Gain [dB]	5.79
Radiated Power [dBm]	9.46
Radiation Efficiency	0.88
S_{11} [dB]	-35 @ 24 GHz
HPBW	86°

Table 4: Chosen patch element characteristics

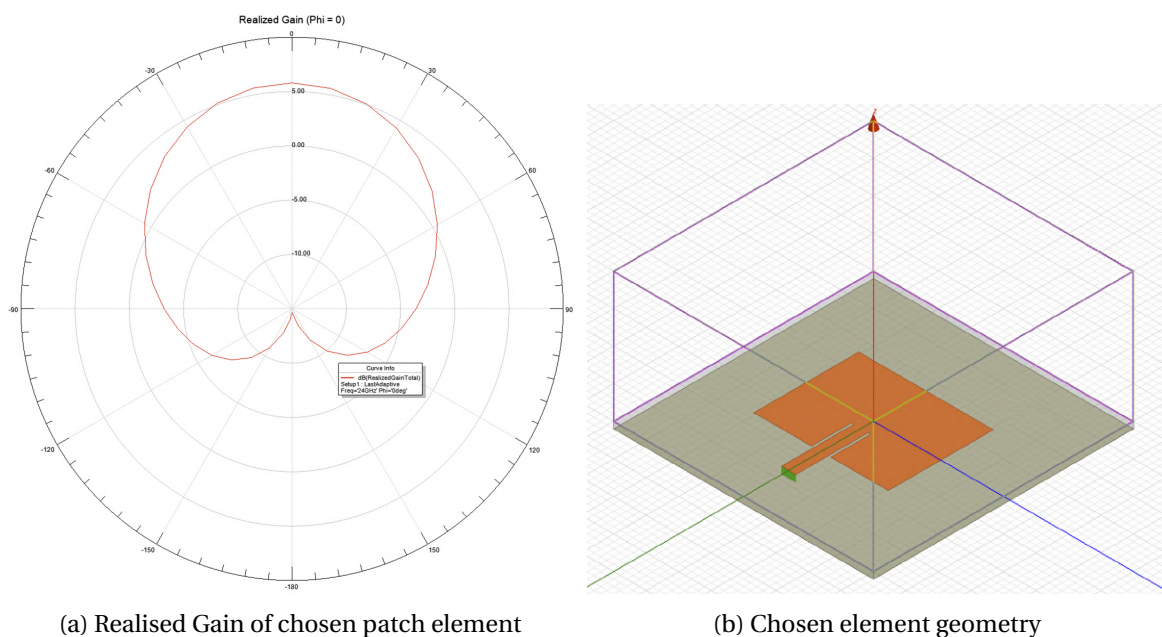(a) Realised Gain of chosen patch element

(b) Chosen element geometry

Fig. 5: Chosen element

4.2 Array factor

The normalized antenna factor for a planar NxM array is given by [12, p. 351] :

$$AF_n(\theta,\phi) = \frac{1}{M}\frac{\sin\left(\frac{M}{2}\Psi_x\right)}{\sin\left(\frac{\Psi_x}{2}\right)} \cdot \frac{1}{N}\frac{\sin\left(\frac{N}{2}\Psi_y\right)}{\sin\left(\frac{\Psi_y}{2}\right)} \tag{4.1}$$

With

$$\Psi_x = kd_x\sin\theta\cos\phi + \beta_x \tag{4.2}$$

$$\Psi_y = kd_y\sin\theta\cos\phi + \beta_y \tag{4.3}$$

This is essentially a combination of two linear arrays respectively in the E-Plane and H-Plane of the antenna. In order to select a good number of elements in the E-Plane to achieve the desired HPBW as seen in section 2.3, we must find N such that

$$AF_n(\theta,\phi = 0) = \frac{1}{N}\frac{\sin\left(\frac{N}{2}\Psi_y\right)}{\sin\left(\frac{\Psi_y}{2}\right)} = \sqrt{\frac{1}{2}} \tag{4.4}$$

Note the square root comes from the fact the array factor is related to amplitude, so half the power equates to $\sqrt{\frac{1}{2}}$ of the amplitude.

For the chosen feeding method (see section 4.4) and since no beam-forming is necessary at this point, we choose to have constant phase in both axis so $\beta_x = \beta_y = 0$. To avoid grating lobes we set $d_x = d_y = \frac{\lambda}{2}$. This yields:

$$\Psi_y = \Psi_x = k\frac{\lambda}{2}\sin\theta\cos\phi = \pi\sin\theta\cos\phi \tag{4.5}$$

To find N for a 12 degree HPBW in the E-Plane, we write:

$$AF_n(\theta = 6°,\phi = 0) = \frac{1}{N}\frac{\sin\left(\pi\frac{N}{2}\sin(6°)\right)}{\sin\left(\frac{\pi}{2}\sin(6°)\right)} = \sqrt{\frac{1}{2}} \Rightarrow N = 8.52 \tag{4.6}$$

Because the feeding method requires N to be a power of 2 (and of course a round number), we choose the closest power of two to the computed value of N and set N=8.

While we have seen that HPBW in the H-Plane has no apparent effect on the measurement error (assuming perfect mounting), we choose M=2 elements in the H-Plane, yielding a beam width of about 60° to avoid a too large HPBW in this axis causing unwanted reflections. The normalized AF for different numbers of elements is shown in figure 6.

4.3 Simulated array

Both 2x4 and 2x8 arrays were simulated before starting work on the feeding scheme to confirm the array dimensions. As can be seen in figure 7, the desired HPBW is acheived with a 2x8 array, and only a small effect of the coupling can be observed, without the Sidelobe Level (SLL) being too high.
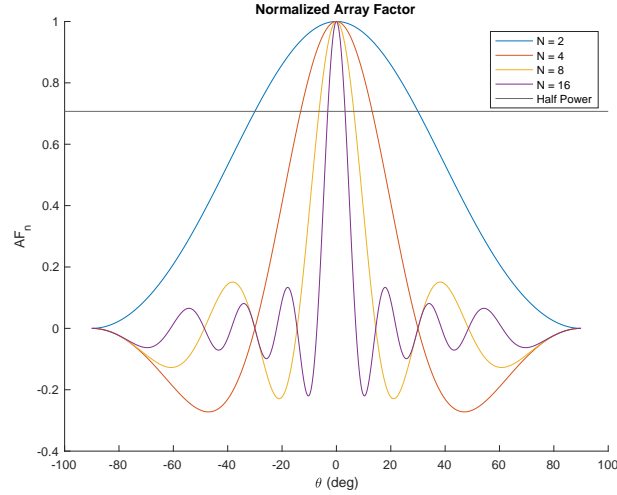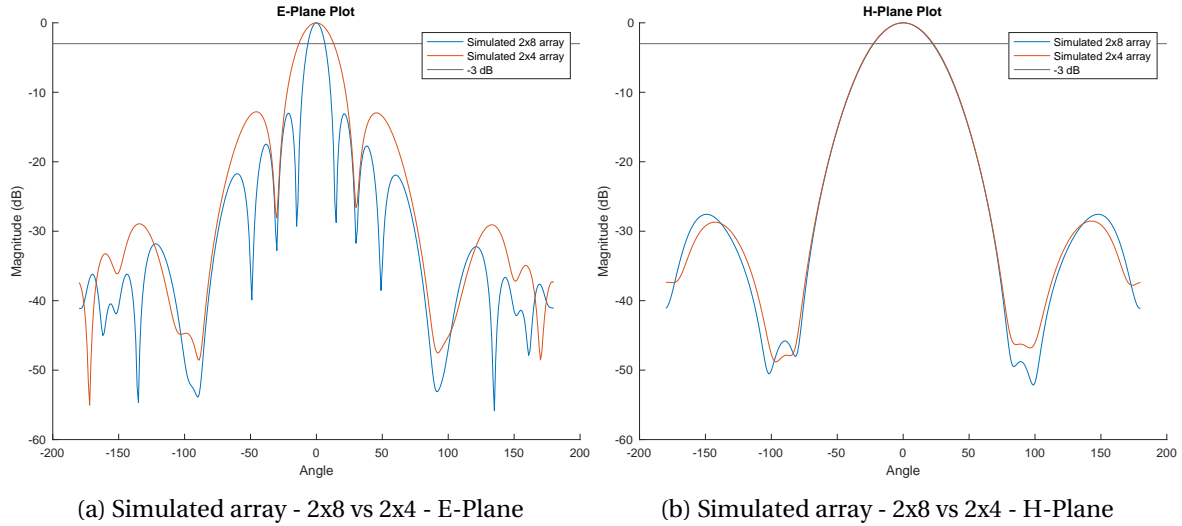
Fig. 6: Normalized Array Factor for different number of elements

(a) Simulated array - 2x8 vs 2x4 - E-Plane

(b) Simulated array - 2x8 vs 2x4 - H-Plane

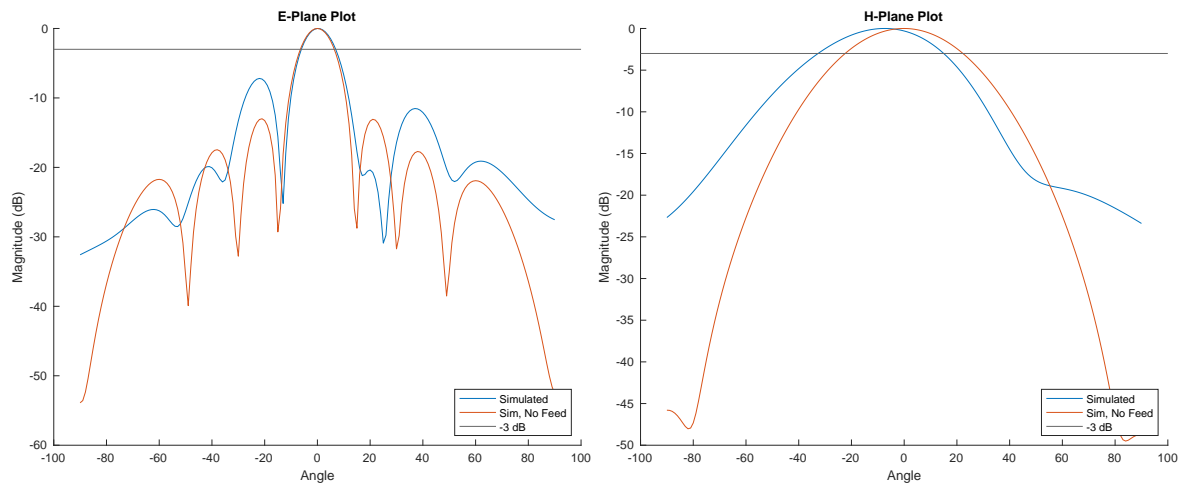Fig. 7: Simulated array - 2x8 vs 2x4

4.4 Feeding Scheme

In order to equally divide power between each element, corporate feeding is used. The source 50Ω ($W_{50} = 0.44$mm) line is split into two 100Ω ($W_{100} = 0.11$mm) lines, and then a 70Ω ($W_{70} = 0.22$mm) quarter wave transformer is used to match each line back to 50Ω (see fig. 8). This division and matching is continued until all the elements are fed.

The results of the simulation of the feeding scheme (on its own) are indicated in table 5. As we can see the feeding method equally divides power ($S_{12} \approx S_{13} \approx -3$dB) and only has small reflection ($S_{11} < 20$dB).

S_{11} [dB]	-20.04
S_{12} [dB]	-3.12
S_{13} [dB]	-3.16

Table 5: Simulation results of feeding scheme

Fig. 8: Array Feeding Scheme

4.5 Complete Array

The results of the complete 2x8 array simulations including feeding are shown in figures 9 and 10. As we can see the feeding network has a clear impact on radiation pattern, but the SLL remains close to -10 dB. Due to time constraints and the desire to manufacture a first prototype the feeding network was clearly not optimal. Nonetheless the antenna is matched quite close to the desired frequency of 24 GHz with a S_{11} of around -13.5 dB, and has a satisfactory HPBW and realized gain. Due to manufacturing tolerances, the inset feed spacing had to be readjusted to be greater than 100 μm, without any significant effect on the radiation pattern.
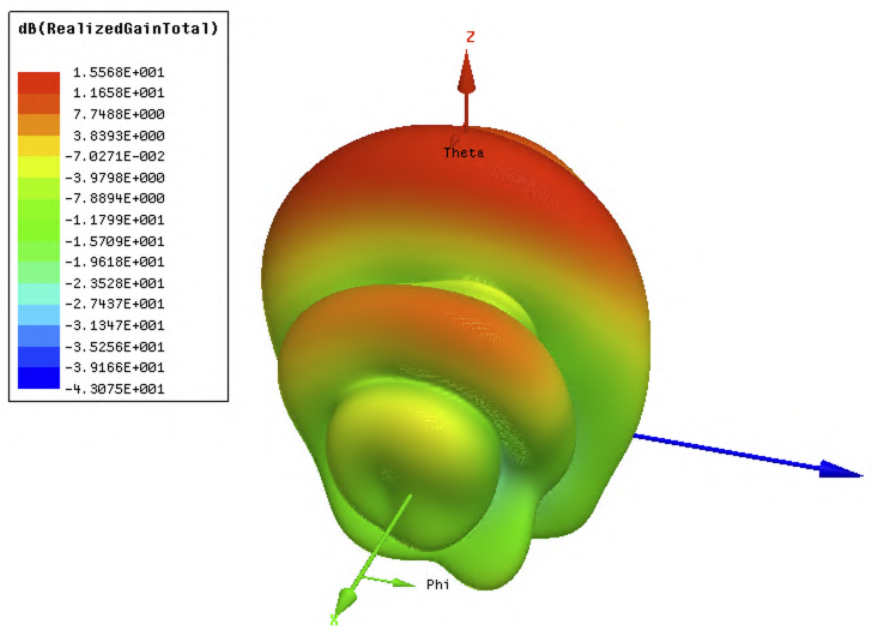

Fig. 9: S_{11} of simulated complete array

(a) Radiation Pattern - E-Plane

(b) Radiation Pattern - H-Plane

(c) Realized Gain of complete array

Fig. 10: Complete array simulation results

5 Experimental validation

With the prototype manufactured, measurements of the antenna radiation pattern were performed in an anechoic chamber. The Antenna Under Test (AUT) was mounted on a rotating platform (figure 11(b)) and a reference horn antenna was placed opposite to it (fig. 11(a)) at a distance of around 1m (fig. 11(c)). An amplifier was connected to the AUT and the antennas were connected to an Agilent E8361A Network Analyzer in order to measure the S_{12} and therefore the AUT's radiation pattern. Since a gain measurement was not the main focus at this time, and a calibrated measurement including the reference antenna characteristics was not possible within the project timeframe, only the radiation pattern in both the E-Plane and H-Plane were measured. The measurements are shown in figure 12.

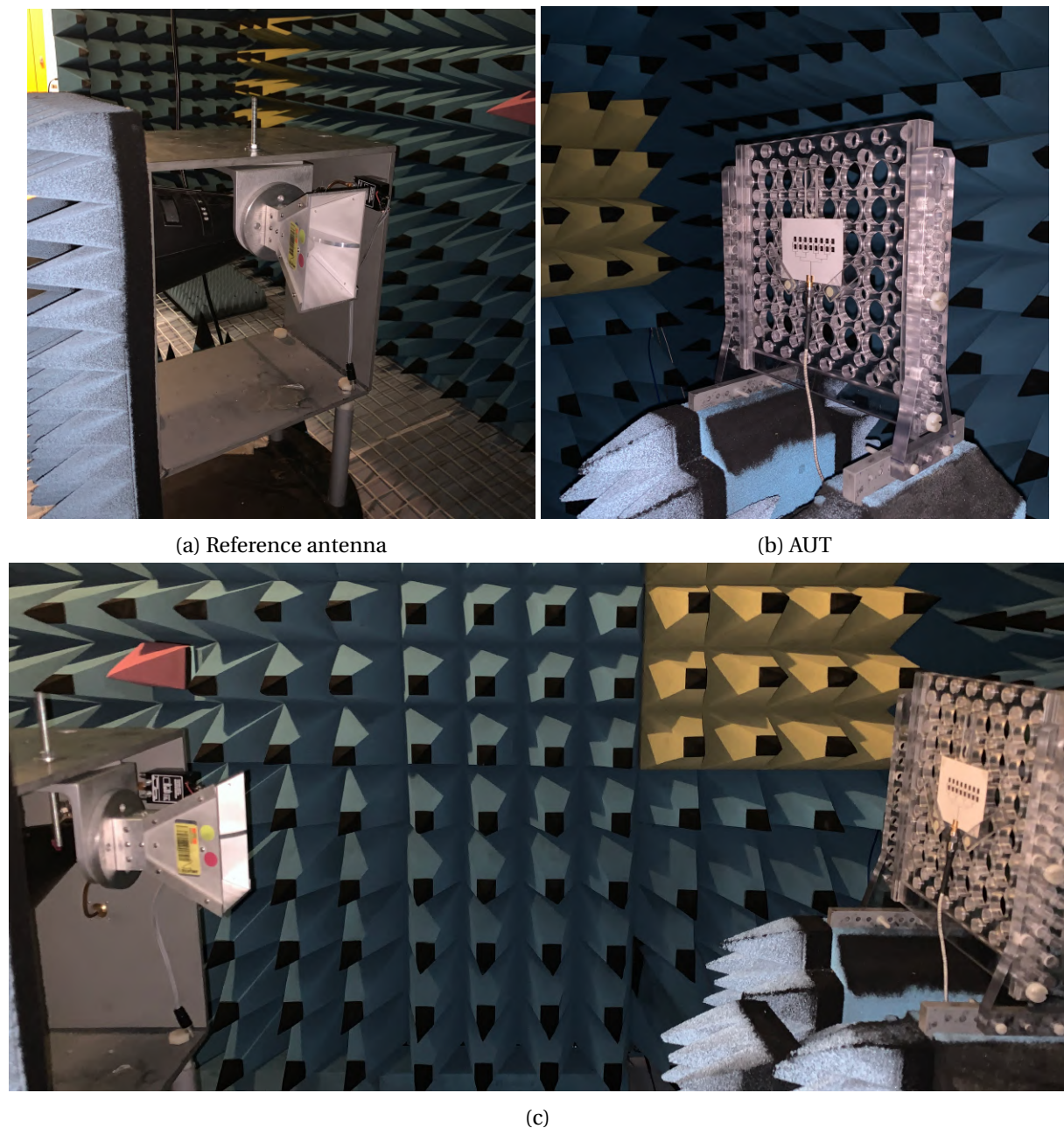(a) Reference antenna   (b) AUT


(c)

Fig. 11: Measurement setup

The measured data showed some high frequency ripples, possibly due to multiple reflections in the antenna and measurement setup, so the results were low-pass filtered with a normalized passband

frequency of 0.2. Nonetheless we can see that the manufactured antenna follows the simulation quite close near the center as shown in figure 12(c), and exhibits a HPBW of around 12° in the E-Plane as desired, with a SLL similar to the simulated array.
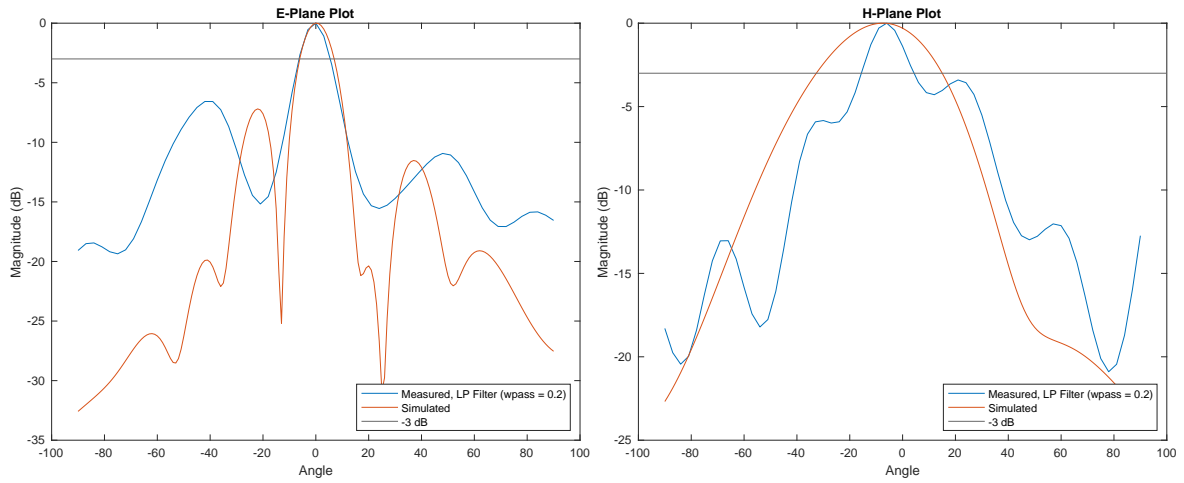
(a) Measured vs Simulated array - E-Plane

(b) Measured vs Simulated array - H-Plane
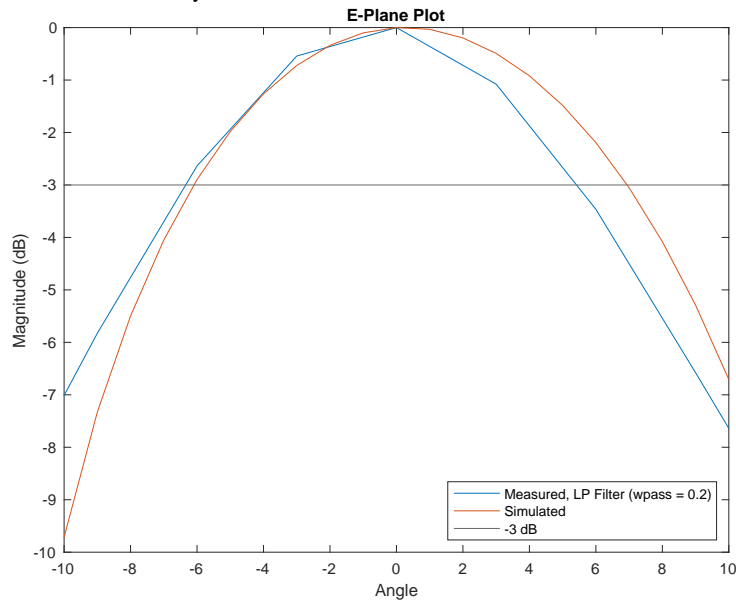
(c) Measured vs Simulated array - E-Plane Zoom

Fig. 12: Measured vs Simulated 2x8 Array

6 Conclusions

In conclusion, we have seen that a microwave patch antenna array can be designed to limit the relative speed measurement error of a vehicular speed measurement RADAR, with promising results. Based on this work a full system can be implemented, with the hopes of contributing an accurate measurement of speed for use in not only the control algorithms but also the fully autonomous vehicles from EPFL Racing Team. This project allowed me to push the limits of my understanding in the field of microwaves, and the subtle ways such systems behave, and I look forward for the continued work on this type of system within the team.

6.1 Future work

Once a full system implementing the RADAR MMIC, supporting circuitry and possibly a more optimized array is designed and manufactured, the antenna model can be used for very precise signal processing [3]. Building two of such systems and mounting them so that one faces forward and the other backwards (also called a Janus configuration), can allow even better accuracy by compensating for vehicle tilt [6]. Finally, a higher frequency of 77GHz can be explored for better measurements on wet or icy roads [8] and to allow for denser arrays, further reducing the HPBW.

6.2 Acknowledgements

7 Appendix

MATLAB code for figure 2:

```matlab
% Parameters
alpha_deg = linspace(5, 10, 1000); % Beam angle in degrees
delta_theta_deg = linspace(10, 14, 1000); % HPBW in degrees

% Convert alpha and delta theta to radians
alpha = alpha_deg * pi/180;
delta_theta = delta_theta_deg * pi/180;

% Initialize relative error matrix
relative_error = zeros(length(alpha_deg), length(delta_theta_deg));

% Calculate relative error for each combination of alpha and delta
   theta
for i = 1:length(alpha)
    for j = 1:length(delta_theta)
        % Calculate relative error
        relative_error(i, j) = delta_theta(j) * tan(alpha(i));
    end
end

% Plot the relative error as a 2D color matrix
figure;
imagesc(delta_theta_deg, alpha_deg, relative_error);
set(gca, 'YDir', 'normal');
xlabel('\Delta\theta (degrees)');
ylabel('\alpha (degrees)');
colormap turbo
a = colorbar;
a.Label.String = 'Relative speed error';
%title('Relative Error vs. \alpha and \Delta\theta');

hold on;

% Plot the line where alpha is equal to half delta theta
half_line = linspace(0, 90, 1000);
plot(half_line, half_line/2, 'k--', 'LineWidth', 2);

% Plot the contour for relative error below 1/33.3
contour(delta_theta_deg, alpha_deg, relative_error, [1/33.3
   1/33.3], 'LineColor', 'black', 'LineWidth', 2);

hold off;

legend('\alpha = \Delta\theta / 2', 'Relative Speed Error = 1/33.3'
   , 'Location', 'southeast');
saveas(gcf,'relative_error','epsc')
```

19

MATLAB code for figure 6:

```matlab
clear all; close all; clc;

% Define the function
AF = @(N, theta) (1./N) .* (sin(pi .* (N./2) .* sin(theta))) ./ (
   sin((pi/2) .* sin(theta)));

% Define the values of N
N = [2, 4, 8, 16]; % Use a vector to specify multiple values of N

% Define the range of theta values
theta = linspace(-pi/2, pi/2, 1000);

% Plot the function for each value of N
figure;
hold on;
for i = 1:length(N)
    y = AF(N(i), theta);
    plot(rad2deg(theta), y, 'DisplayName', sprintf('N = %d', N(i)))
        ;
end

yline(sqrt(1/2), 'DisplayName', 'Half Power')
hold off;
legend;

title('Normalized Array Factor')
ylabel("AF_n")
xlabel("\theta (deg)")

saveas(gcf,'ArrayFactor','epsc')
```

MATLAB code for figure 7:

```
clear all; close all; clc;



radPatternNoFeed_2x8 = readtable('rad_pat_nofeed.csv');
radPatternNoFeed_2x4 = readtable('2x4.csv');

% y = EPlane.results(:, 2);
% y_shifted = y - max(y);

% E Plane plot
figure
hold on
plot(radPatternNoFeed_2x8{:, 1}, radPatternNoFeed_2x8{:, 2}, "
    DisplayName", "Simulated 2x8 array") % Simulated values
plot(radPatternNoFeed_2x4{:, 1}, radPatternNoFeed_2x4{:, 2}, "
    DisplayName", "Simulated 2x4 array") % Simulated values
legend
yline(-3,"DisplayName", "-3 dB")
title('E-Plane Plot')
xlabel("Angle")
ylabel("Magnitude (dB)")
%xlim([-10 10])
saveas(gcf,'array_size_comparison_E','epsc')

% H Plane plot
figure
hold on
plot(radPatternNoFeed_2x8{:, 1}, radPatternNoFeed_2x8{:, 3}, "
    DisplayName", "Simulated 2x8 array") % Simulated values
plot(radPatternNoFeed_2x4{:, 1}, radPatternNoFeed_2x4{:, 3}, "
    DisplayName", "Simulated 2x4 array") % Simulated values
yline(-3,"DisplayName", "-3 dB")
legend
title('H-Plane Plot')
xlabel("Angle")
ylabel("Magnitude (dB)")
%xlim([-10 10])
saveas(gcf,'array_size_comparison_H','epsc')
```

MATLAB code for figure 9:

```
clear all; close all; clc;



s11_2x8_values = readtable('2x8_feed_s11.csv');

% y = EPlane.results(:, 2);
% y_shifted = y - max(y);

% E Plane plot
figure
hold on
plot(s11_2x8_values{:, 1}, s11_2x8_values{:, 2}) % Simulated values
%legend
%yline(-3,"DisplayName", "-3 dB")
title('S_{11} of simulated 2x8 array with corporate feeding')
xlabel("Frequency (GHz)")
ylabel("|S_{11}| (dB)")
%xlim([-10 10])
saveas(gcf,'s11_2x8_feed','epsc')
```

MATLAB code for figure 10

```
clear all; close all; clc;

EPlane = load('Meas_06062023/mmW_24GHz_Radar_8x2_Array_E_plane_3deg
    .mat');
HPlane = load('Meas_06062023/mmW_24GHz_Radar_8x2_Array_H_plane_3deg
    .mat');

radPattern = readtable('Array2x8_RadiationPattern_trimmed');
radPatternNoFeed = readtable('rad_pat_nofeed_trimmed.csv');

wpass_Eplane = 0.2;
y_lp = lowpass(EPlane.results(:, 2), wpass_Eplane);
y_shifted_lp = y_lp - max(y_lp);

% y = EPlane.results(:, 2);
% y_shifted = y - max(y);

% E Plane plot
figure
displayName = sprintf("Measured, LP Filter (wpass = %.1f)",
    wpass_Eplane);
%plot(EPlane.results(:, 1), y_shifted_lp, "DisplayName",
    displayName) % Interpolated Measurements
hold on
%plot(EPlane.results(:, 1), y_shifted, "DisplayName", "Raw") % Raw
plot(radPattern{:, 1}, radPattern{:, 2}, "DisplayName", "Simulated
    ") % Simulated values
plot(radPatternNoFeed{:, 1}, radPatternNoFeed{:, 2}, "DisplayName",
     "Sim, No Feed") % Simulated values no feed
yline(-3,"DisplayName", "-3 dB")
legend('Location','southeast')
title('E-Plane Plot')
xlabel("Angle")
ylabel("Magnitude (dB)")
%xlim([-10 10])
saveas(gcf,'sim_vs_real_E','epsc')

% H Plane plot
wpass_Hplane = wpass_Eplane;
y = lowpass(HPlane.results(:, 2), wpass_Hplane);
y_shifted = y - max(y);

figure
displayName = sprintf("Measured, LP Filter (wpass = %.1f)",
    wpass_Hplane);
%plot(HPlane.results(:, 1), y_shifted, "DisplayName", displayName);
hold on
plot(radPattern{:, 1}, radPattern{:, 3}, "DisplayName", "Simulated
    ") % Simulated values
plot(radPatternNoFeed{:, 1}, radPatternNoFeed{:, 3}, "DisplayName",
```

```matlab
    "Sim, No Feed") % Simulated values no feed
yline(-3, "DisplayName", "-3 dB")
title('H-Plane Plot')
xlabel("Angle")
ylabel("Magnitude (dB)")
legend('Location','southeast')

saveas(gcf,'sim_vs_real_H','epsc')
```

8 References

[1] R. Rasshofer and E. Biebl, "Advanced millimeterwave speed sensing system based on low-cost active integrated antennas," in *1999 IEEE MTT-S International Microwave Symposium Digest (Cat. No.99CH36282)*, vol. 1. Anaheim, CA, USA: IEEE, 1999, pp. 285–288. [Online]. Available: http://ieeexplore.ieee.org/document/779476/

[2] Seoktae Kim and Cam Nguyen, "Millimeter-wave doppler velocimetry for low-velocity measurement," in *2004 IEEE MTT-S International Microwave Symposium Digest (IEEE Cat. No.04CH37535)*, vol. 2. Forth Worth, TX, USA: IEEE, 2004, pp. 663–666. [Online]. Available: http://ieeexplore.ieee.org/document/1336074/

[3] J. Dybedal, "Doppler Radar Speed Measurement Based On A 24 GHz Radar Sensor." [Online]. Available: https://www.researchgate.net/publication/306290600_Doppler_Radar_Speed_Measurement_Based_On_A_24_GHz_Radar_Sensor

[4] K. K. M. Shariff, E. Hoare, L. Daniel, M. Antoniou, and M. Cherniakov, "Comparison of Adaptive Spectral Estimation for Vehicle Speed Measurement with Radar Sensors," *Sensors*, vol. 17, no. 4, p. 751, Apr. 2017. [Online]. Available: http://www.mdpi.com/1424-8220/17/4/751

[5] F. B. Berger, "The Nature of Doppler Velocity Measurement," *IRE Transactions on Aeronautical and Navigational Electronics*, vol. ANE-4, no. 3, pp. 103–112, Sep. 1957. [Online]. Available: http://ieeexplore.ieee.org/document/4201534/

[6] K. K. M. Shariff, Z. Awang, I. Pasya, and S. A. M. Al Junid, "Theoretical Accuracy Analysis of a 4-Beam Speed- Over-Ground Radar on Uneven Surface," in *2018 IEEE International RF and Microwave Conference (RFM)*. Penang, Malaysia: IEEE, Dec. 2018, pp. 325–328. [Online]. Available: https://ieeexplore.ieee.org/document/8846527/

[7] F. Gardiol, *Hyperfréquences*, ser. Traité d'électricité de l'Ecole polytechnique fédérale de Lausanne vol. 13. St-Saphorin: Georgi, 1981, vol. 13.

[8] V. Viikari, T. Varpula, and M. Kantanen, "automotive radar technology for detecting road conditions. Backscattering properties of dry, wet, and icy asphalt," in *2008 European Radar Conference*, Oct. 2008, pp. 276–279. [Online]. Available: https://ieeexplore.ieee.org/document/4760855

[9] E. Klinefelter and J. A. Nanzer, "Millimeter-Wave Interferometric Radar for Speed-Over-Ground Estimation," in *2020 IEEE/MTT-S International Microwave Symposium (IMS)*, Aug. 2020, pp. 1023–1026, iSSN: 2576-7216.

[10] T. M. Hyltin, T. D. Fuchser, H. B. Tyson, and W. R. Regueiro, "Vehicular Radar Speedometer," *SAE Transactions*, vol. 82, pp. 473–502, 1973, publisher: SAE International. [Online]. Available: https://www.jstor.org/stable/44716328

[11] W. Kleinhempel, D. Bergmann, and W. Stammler, "Speed measure of vehicles with on-board Doppler radar," in *92 International Conference on Radar*, Oct. 1992, pp. 284–287.

[12] C. A. Balanis, *Antenna theory: analysis and design*, 3rd ed. Hoboken, NJ: John Wiley, 2005.

[13] "Formula Student Rules 2023." [Online]. Available: https://www.formulastudent.de/fileadmin/user_upload/all/2023/rules/FS-Rules_2023_v1.1.pdf

[14] "Infineon BGT24LTR11N16 Datasheet." [Online]. Available: https://www.infineon.com/dgdl/Infineon-BGT24LTR11N16-DataSheet-v01_03-EN.pdf?fileId=5546d4625696ed7601569d2ae3a9158a

[15] K. Scheiwiller, "Ground speed sensor," Tech. Rep., Jan. 2023.

[16] "Non-contact optical sensors Correvit SF-Motion | Kistler." [Online]. Available: https://www.kistler.com/DE/en/cp/non-contact-optical-sensors-correvit-sf-motion-2059a/P0000168

[17] Y. Antille, E. Gubler, and J.-M. Gruber, "Ground Speed Measuring System for Autonomous Vehicles:," in *Proceedings of the 18th International Conference on Informatics in Control, Automation and Robotics.* Online Streaming, — Select a Country —: SCITEPRESS - Science and Technology Publications, 2021, pp. 661–668. [Online]. Available: https://www.scitepress.org/DigitalLibrary/Link.aspx?doi=10.5220/0010543106610668

[18] M. A. Richards, J. Scheer, W. A. Holm, and W. L. Melvin, Eds., *Principles of modern radar.* Raleigh, NC: SciTech Pub, 2010.